Received: 23 May 2021 | Revised: 16 September 2021 | Accepted: 30 September 2021

IET Generation, Transmission & Distribution

DOI: 10.1049/gtd2.12384

The Institution of Engineering and Technology WILEY

ORIGINAL RESEARCH PAPER

Higher-order sliding mode current controller for grid-connected distributed energy resources with LCL filters under unknown grid voltage conditions

Mostafa Barzegar-Kalashani[1] | **Behrouz Tousi**[1] | **Md Apel Mahmud**[2,3] | **Mohammad Farhadi-Kangarlu**[1]

[1] Faculty of Electrical and Computer Engineering, Urmia University, Urmia, Iran

[2] Electrical Power and Energy Systems Research Lab (EPESRL), School of Engineering, Deakin University, Waurn Ponds, Australia

[3] Faculty of Engineering and Environment, Northumbria University Newcastle, Tyne & Wear, UK

Correspondence
Behrouz Tousi, Faculty of Electrical and Computer Engineering, Urmia University, Urmia, Iran.
Email: b.tousi@urmia.ac.ir

Abstract

The control of the current injected into the grid with lower harmonics is considered as one of the most important issues for the grid integration of distributed energy resources (DERs). The unbalances and harmonics in the grid voltage usually pollute the current injected into the grid due to the power electronic interfaces, for example, inverters. To address such problems, the present paper proposes a nonlinear higher order sliding mode controller (HOSMC) for grid-connected three-phase inverters with LCL filters in order to control the current injected into grid and improve the power quality. The proposed current controller injects the desired current into the grid with lower values of total harmonic distortions (THDs) under any grid voltage condition as well as it reduces the harmonics in the grid voltage. Apart from these, the proposed scheme is developed to provide robustness against parametric uncertainties where these uncertainties are modeled using the Taylor series expansion method. Finally, the performance of the system is evaluated using processor-in-loop (PIL) simulations via MATLAB/Simulink platform through the implementation on a system considering the capacity of the DER as 2 kVA per phase and compared with other existing control strategies.

1 | INTRODUCTION

Power electronic interfaces with different types of filters are considered as integral parts for connecting renewable energy-based distributed energy resources (DERs) with the main power grid [1, 2]. Since most of DERs generate DC power, voltage source inverters (VSIs) are employed to convert the DC power into the AC power. These inverters can be either single- or three-phase depending on the application. Filters are used at the output of these inverters in order to improve the power quality which usually deteriorates by the switching actions. The most commonly used filters with power electronic interfaces are *L* or LCL filters though LC filters are used in some cases [3]. The *L* filter with the attenuation of 20 dB/decade can be easily used for converters with the high switching frequency [3, 4]. However, the large amount of the filter inductance affects the dynamic characteristics and efficiency of the system. An LCL filter with the attenuation of 60 dB/decade is an alternative way to resolve the drawbacks of *L* filters. The third-order LCL filter has the ability to decrease the total harmonic distortion (THD) in the output current of the inverter using the lower switching frequency with better attenuations and reduced costs as well as sizes as the total inductance is less than *L* filters [1–6]. The THD is a measurement of the distortion in a signal and it defines the purity of a sinusoidal waveform. However, the control of current injected into the grid with the LCL filter at the output-side of the inverter is more complex as the order of the system becomes higher and requires further studies.

In recent years, different current control schemes using linear and nonlinear techniques have been designed for both single- and three-phase grid-connected inverters having *L* and LCL filters at the output of these inverters. Several current controllers such as the proportional-integral (PI) controller [7], proportional-resonant (PR) controller [8], hybrid grid voltage

feed-forward with the multi-harmonic resonant (HR) controller [9], deadbeat controller [10], and repetitive controller [11] have been proposed over few last decades. However, these linear controllers have some major drawbacks including low speed in response, higher steady-state error, failing in removing disturbances' effects which bring vital challenges in modern microgrids consisting of different uncertainties and main grid disturbances.

Due to major drawbacks of the linear control approaches, the nonlinear control strategies specifically the variable structure control scheme have been developed in which the sliding mode controller (SMC) is widely used for power converter applications. The SMC with multi-resonant sliding surfaces [12] and SMC with the double-band hysteresis scheme [13] are employed for single-phase inverters. On the other hand, the sliding mode harmonic compensation (SMHC) scheme [14]; SMC with the PR (SMC+PR) scheme in both natural and rotating dq frames [15]; discrete-time SMC (DSMC) with the PR (DSMC+PR) controller for active damping [16]; and SMC with the Kalman filter estimator (SMC+KFE) [17] are employed for three phase grid-connected inverters. The sliding mode control strategies in [12] and [15] are similar apart from their applications in single- and three-phase grid-connected inverters. The SMCs in [12] and [15] effectively reduce the harmonics in the grid current along with the number of measurement sensors. However, these controllers still suffer from the chattering phenomenon as these are not designed by considering the higher-order sliding surface. Hence, the unmodeled dynamics are excited with these lower-order SMCs. The SMHC scheme in [14] is a non-selective harmonic compensation approach which effectively decreases the computational burden in comparison with other selective conventional techniques. The SMHC scheme in [14] has two parts: one is the harmonic detector while the other one is the sliding mode harmonic current controller. In [14], the SMHC scheme is employed for a three-phased grid-connected inverter under distorted grid voltage conditions from where it is found that it exhibits low chattering phenomenon and provides robustness against disturbances. However, the value of THDs in the injected current into the grid is too high. Since the SMHC scheme combines the conventional PI controller with the nonlinear SMC, it becomes more complicated and causes non-finite-time convergence similar to that of [12, 15]. The DSMC+PR in [16] is a robust hybrid discrete controller which uses a virtual resistor in order to eliminate the effects of uncertainties and reduce THDs in the grid current. However, the DSMC+PR uses more voltage and current sensors as compared to other existing SMCs which decreases the overall reliability of the system. In [17], the SMC is used with a KFE to reduce the number of measurement sensors and improve the current tracking performance as compared to the conventional SMC. However, the SMC+KFE uses larger values of filter parameters and there still exists the chattering phenomenon. In [18], two robust SMCs are designed based on super-twisting algorithms for *L*- and *LC*- filtered single-phase inverters in islanded/anti-islanded operation modes with considering parametric uncertainties in which the presented algorithms are robust against disturbances, however, using low-order filters reduces the attenuation gain as long as the effects of harmonics are not eliminated carefully as the low-order sliding surfaces are used.

In light of literature so far presented in this paper, the main problems (excluding the chattering phenomenon) with existing SMCs for single- or three-phase grid-connected in inverters are the robustness against parametric uncertainties, distortion in the grid voltage, THDs in the grid current, and unbalances in the grid voltage. The existing SMCs do not provide solutions for all these problems. As evidenced from the theoretical analysis and different applications, it is seen that the higher-order sliding mode controller (HOSMC) is considered as an alternative way to overcome chattering problems and improving the performance of the system under severe disturbances [19–22]. Though the HOSMCs in [20, 22] reduces the chattering problems, these controllers are designed based on the feedback linearized models of nonlinear systems and such models are obtained by canceling useful nonlinearities of the system. The controllers, which are designed based on these feedback linearized models, are highly sensitive to parameter variations and the controllers in [20, 22] consider the perturbations in parameters only for the feedback linearized model where some parameters do not appear due to the cancelation of nonlinearities. Hence, these controllers are unable to provide robustness against all parametric uncertainties. An integral-HOSMC is designed in [23] for T-type four-wire inverter for islanded DERs. The presented controller in [23] is robust against different load changes, however, the model of the system have not considered the parametric uncertainties in order to design the controllers' coefficients, accurately.

This paper focuses to design a HOSMC for three-phase grid-connected inverters with LCL filters in order to effectively facilitate the integration of DERs. The robustness of SMCs against parametric uncertainties depends on the modeling of these uncertainties. In this work, the parametric uncertainties are considered for all parameters and modeled through the Taylor series expansion method while the proposed HOSMC is designed based on such models. The performance of the controller is evaluated by considering the unbalances and distortions in the grid voltage and PIL simulation studies are carried out to validate performance of the proposed scheme. The PIL simulation results clearly demonstrate the effectiveness of the proposed scheme against parametric uncertainties, distortion in the grid voltage, THDs in the grid current, and unbalances in the grid voltage. Comparisons are also made with different existing methods in order to analyze the superiority of the proposed scheme.

The rest of the paper is organized as follows. Section 2 describes the modeling of the three-phase grid-connected inverter with an LCL filter. In Section 3, the design procedure of the proposed HOSMC is explained along with the uncertainty modeling and stability analysis. The performance evaluation of the proposed controller under different grid voltage conditions and uncertainties filter parameters including comparisons with other methods is discussed in Section 4 through PIL simulation studies. Finally, Section 5 provides concluding remarks

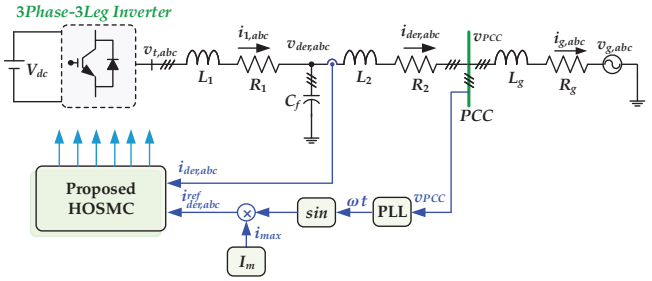

FIGURE 1 The schematic diagram of a grid-connected DER unit through a three-phase three-leg inverter with an LCL filter

highlighting the main finding of this work along with comments on future works.

2 | SYSTEM MODELING

Figure 1 shows the configuration of a grid-connected DER through a three-phase three-leg inverter with an LCL filter along with a closed-loop control scheme. The three-phase inverter consists of six power switches which properly triggered using pulsed width modulation (PWM) signals. In addition, the employed LCL filter consists of an inverter side inductor (L_1) and resistor (R_1); a shunt filter capacitor (C_f); a line inductor (L_2) and resistor (R_2); and the grid side inductor (L_g) and resistor (R_g).

The dynamical model of this grid-connected DER can be obtained by applying Kirchhoff's voltage and current laws (i.e. KVL and KCL) and represented through following three equations:

$$L_1 \frac{di_{1,p}}{dt} = v_{t,p} - v_{der,p} - R_1 i_{1,p}, \tag{1}$$

$$C_f \frac{dv_{der,p}}{dt} = i_{1,p} - i_{der,p}, \tag{2}$$

$$L_2 \frac{di_{der,p}}{dt} = v_{der,p} - R_2 i_{der,p} - v_{pcc,p}, \tag{3}$$

where the subscript p indicates three different phases, that is, a, b, and c; and $i_{1,p}$, $v_{t,p}$, $v_{der,p}$, $i_{der,p}$, and $v_{pcc,p}$ represent the inverter-side current, control signal; voltage of the DER unit; line current at the output-side of the LCL filter, and voltage at point of common coupling (PCC), respectively. It is worth to mention that a PLL is used to the DER with the grid and it is assumed that the dynamics of the PLL is faster than that of the LCL filter. Hence, the dynamic of the PLL is ignored in the overall dynamical model of the inverter. However, the existence of the unbalances and disturbances in the grid voltage as well as in the frequency might cause the instability of the dynamics of the PLL. Recently, it is revealed that the unbalances and harmonics in the grid voltage do not have special effects on the overall operation of the system [24] which is another reason to neglect the dynamics of the PLL. Equations (1)–(3) can be combined together and expressed in the form of the following third-order differential equation:

$$\begin{aligned}\frac{d^3 i_{der,p}}{dt^3} = {} & \frac{1}{L_1 L_2 C_f} v_{t,p} - \left(\frac{R_1}{L_1} + \frac{R_2}{L_2}\right) \frac{d^2 i_{der,p}}{dt^2} \\ & - \left(\frac{1}{L_1 C_f} + \frac{R_1 R_2}{L_1 L_2} + \frac{1}{L_2 C_f}\right) \frac{d i_{der,p}}{dt} - \frac{R_1 + R_2}{L_1 L_2 C_f} i_{der,p} \\ & - \left(\frac{1}{L_2} \frac{d^2 v_{pcc,p}}{dt^2} + \frac{R_1}{L_1 L_2} \frac{dv_{pcc,p}}{dt} + \frac{1}{L_1 L_2 C_f} v_{pcc,p}\right).\end{aligned} \tag{4}$$

Equation (4) which defines the third-order model of a grid-connected DER with a three-phase three-leg inverter and an LCL filter which comprised different parameters and there exist uncertainties in these parameters. Since the proposed HOSMC controller is designed based on the state-space model in order to provide robustness against parametric uncertainties, the state-space and parametric uncertainty modeling are discussed in the following section.

3 | PROPOSED CONTROLLER DESIGN

This section focuses to develop the state-space and uncertainty modeling of the dynamical model in order to design the proposed HOSMC. At the beginning, the state-space model is obtained by employing the error signal for the current at the output-side of the LCL filter, that is, $i_{der,p}$. The parametric uncertainties are then modeled based on the Taylor series expansion method and finally, the controller is designed based on the third-order dynamical model with these uncertainties along with the stability analysis. All these are discussed in the following subsections.

3.1 | State-space representation

The error signal ($e_{i_{der,p}}$) for the current ($i_{der,p}$) at the output-side of the LCL filter can be defined as follows:

$$e_{i_{der,p}} = i^{ref}_{der,p} - i_{der,p}, \tag{5}$$

where $i^{ref}_{der,p}$ is the reference value of $i_{der,p}$. The error signal and the first two derivatives of this signal can be specified through the following equations:

$$x_{1,p} = e_{i_{der,p}}, \tag{6}$$

$$x_{2,p} = \frac{de_{i_{der,p}}}{dt} = \dot{x}_{1,p}, \tag{7}$$

$$x_{3,p} = \frac{d^2 e_{i_{der,p}}}{dt^2} = \dot{x}_{2,p}. \tag{8}$$

Now, the chain of integrator equations of the system can be restated as in Equation (9) using $x_{1,p}$, $x_{2,p}$, and $x_{3,p}$ as state variables.

$$\begin{aligned}\dot{x}_{1,p} &= x_{2,p},\\ \dot{x}_{2,p} &= x_{3,p},\\ \dot{x}_{3,p} &= \frac{d^3 i_{der,p}^{ref}}{dt^3} - \frac{d^3 i_{der,p}}{dt^3}.\end{aligned} \tag{9}$$

Substituting the value of $\frac{d^3 i_{der,p}}{dt^3}$ from Equation (4), the expression for $\dot{x}_{3,p}$ in Equation (9) can be written as follows:

$$\begin{aligned}\dot{x}_{3,p} = {} & \frac{d^3 i_{der,p}^{ref}}{dt^3} - \frac{1}{L_1 L_2 C_f} v_{t,p} - \left(\frac{R_1}{L_1} + \frac{R_2}{L_2}\right)\frac{d^2 i_{der,p}}{dt^2}\\ & - \left(\frac{1}{L_1 C_f} + \frac{R_1 R_2}{L_1 L_2} + \frac{1}{L_2 C_f}\right)\frac{d i_{der,p}}{dt} - \frac{R_1 + R_2}{L_1 L_2 C_f} i_{der,p}\\ & - \left(\frac{1}{L_2}\frac{d^2 v_{pcc,p}}{dt^2} + \frac{R_1}{L_1 L_2}\frac{d v_{pcc,p}}{dt} + \frac{1}{L_1 L_2 C_f} v_{pcc,p}\right).\end{aligned} \tag{10}$$

The terms $i_{der,p}$ and $\frac{di_{der,p}}{dt}$ in Equation (10) can be expressed in terms of x_1 and x_2. However, it is avoided in order to shorten the length of this equation as well as other subsequent equations. Equation (10) represents the state-space model of the system for three different phases, that is, *a*, *b*, and *c*. As this equation does not include uncertainties, a detailed analysis considering uncertainties within the parameters of the LCL filter needs to be done as discussed in the following subsection.

3.2 | Modeling of parametric uncertainties

The parameters of the LCL filter appearing in Equation (10) are different from their nominal values during the practical operations. The values of parameters in the LCL filter can be measured accurately. However, the operating conditions of the system change continuously and the parameters of the filter have direct interactions with the grid impedance. The changes in the operating conditions affect the grid impedance which in turn affect the parameters of the LCL filter. Therefore, it is important to consider parametric uncertainties during the controller design process so that the controller has the ability to provide robustness against such uncertainties. The variations in parameters are considered as uncertainties for which Equation (10) is expanded in order to model these. For this purpose, R_{1n}, L_{1n}, R_{2n}, L_{2n}, and C_{fn} are assumed as the nominal values of the filter parameters while R_1, L_1, R_2, L_2, and C_f as corresponding actual values considering the practical operations. If ΔR_1, ΔL_1, ΔR_2, ΔL_2, and ΔC_f are defined as the uncertainties or deviations from their corresponding nominal values R_{1n}, L_{1n}, R_{2n}, L_{2n}, and C_{fn}, respectively; the actual values can be written as $R_1 = R_{1n} + \Delta R_1$, $L_1 = L_{1n} + \Delta L_1$, $R_2 = R_{2n} + \Delta R_2$, $L_2 = L_{2n} + \Delta L_2$, and $C_f = C_{fn} + \Delta C_f$. It is worth to mention that $\Delta R_1 < R_{1n}$, $\Delta L_1 < L_{1n}$, $\Delta R_2 < R_{2n}$, $\Delta L_2 < L_{2n}$, and $\Delta C_f < C_{fn}$. Therefore, Equation (10) can be written as follows:

$$\begin{aligned}\dot{x}_{3,p} = {} & \frac{d^3 i_{der,p}^{ref}}{dt^3} - \alpha_1 v_{t,p} + (\alpha_2 + \alpha_3)\frac{d^2 i_{der,p}}{dt^2}\\ & + (\alpha_4 + \alpha_5 + \alpha_6)\frac{d i_{der,p}}{dt} + \alpha_7 i_{der,p} + \alpha_8 \frac{d^2 v_{pcc,p}}{dt^2}\\ & + \alpha_9 \frac{d v_{pcc,p}}{dt} + \alpha_1 v_{pcc,p},\end{aligned} \tag{11}$$

where the terms α_1 to α_9 in Equation (11) represent the nominal part (i.e. α_{1n} to α_{9n}) and uncertainties parts (i.e. $\Delta\alpha_1$ to $\Delta\alpha_9$) in which the expressions of these terms are provided in Appendix. In these terms, the parametric uncertainties need to be separated and from this point of view, different uncertainty terms in Equation (11) are expanded using Taylor series expansion method and the detailed calculations considering for these terms are provided in Appendix A. Apart from parametric uncertainties, the presented model in Equation (11) consists of measurable disturbance as mismatched disturbance because of grid voltage (i.e. $v_{pcc,p}$) and its derivatives (i.e. $\frac{dv_{pcc,p}}{dt}$ and $\frac{d^2 v_{pcc,p}}{dt^2}$) in which this mismatched disturbance along with its derivatives are bounded in a practical system.

By using Equations (A4), (A9), (A14), (A19), (A24), (A30), (A35), (A39), and (A45) from Appendix A; Equation (11) can be expressed as follows:

$$\begin{aligned}\dot{x}_{3,p} = {} & \frac{d^3 i_{der,p}^{ref}}{dt^3} - (\alpha_{1n} + \Delta\alpha_1) v_{t,p}\\ & + (\alpha_{2n} + \Delta\alpha_2 + \alpha_{3n} + \Delta\alpha_3)\frac{d^2 i_{der,p}}{dt^2}\\ & + (\alpha_{4n} + \Delta\alpha_4 + \alpha_{5n} + \Delta\alpha_5 + \alpha_{6n} + \Delta\alpha_6)\frac{d i_{der,p}}{dt}\\ & + (\alpha_{7n} + \Delta\alpha_7) i_{der,p} + (\alpha_{8n} + \Delta\alpha_8)\frac{d^2 v_{pcc,p}}{dt^2}\\ & + (\alpha_{9n} + \Delta\alpha_9)\frac{d v_{pcc,p}}{dt} + (\alpha_{1n} + \Delta\alpha_1) v_{pcc,p},\end{aligned} \tag{12}$$

in which,

$$|\Delta\alpha_\mu| = \frac{\varepsilon_\mu \times \alpha_{\mu n}}{100}, \tag{13}$$

where $0 \le \varepsilon_\mu \le \varepsilon_{\max}$ shows the percentage of parameters variations from their nominal values in which $\varepsilon_{\max}$ is considered 20 in this paper. The control signal consists of two parts consisting of equivalent signal ($v_{eq,p}$) and reaching control signal ($v_{r,p}$) which is written as follows:

$$v_{t,p} = v_{eq,p} + v_{r,p}. \tag{14}$$

The proposed HOSMC is designed based on the model with uncertainties in Equation (12) as discussed in the following subsection.

3.3 | Proposed HOSMC design

This subsection presents the detailed design process of the proposed HOSMC for the system under study. In order to design the equivalent part of controller, it is suggested that the presented system in Equation (12) does not have parametric uncertainties. The following integral sliding surface can be introduced to design the proposed controller:

$$\sigma_p = x_{3,p} - \int \psi_p dt, \tag{15}$$

where σ_p represents the sliding surfaces for all three phases as p represents phase a, b, and c. In Equation (15), ψ_p is the feedback signal which can be written as follows [20, 22]:

$$\psi_p = -\sum_{i=1}^{3} k_{i,p} \left| x_{i,p} \right|^{\gamma_{i,p}} sgn(x_{i,p}), \tag{16}$$

where $k_{i,p} > 0$ and $0 < \gamma_{i,p} < 1$ are design parameters and sgn is a signum function which can be defined as follows:

$$sgn(\xi) = \begin{cases} +1 & \text{if} \quad \xi > 0 \\ 0 & \text{if} \quad \xi = 0 \\ -1 & \text{if} \quad \xi < 0 \end{cases}. \tag{17}$$

The feedback signal in Equation (16) will ensure globally finite-time stable equilibrium point [20, 22]. In this work, the control parameters, that is, $k_{i,p}$ with $i = 1, 2, 3$ are chosen in such a way that these satisfy the Hurwitz condition for the polynomial $h^3 + k_{i,3}h^2 + k_{i,2}h + k_{i,1}$ so that the nominal part of Equation (12) can be stabilized in the finite time [25]. This means that ψ_p will only ensure the stability of the nominal part of Equation (12) in the finite-time and it cannot guarantee the stability of the system for the uncertainties as represented by Equation (12). Furthermore, it is noticeable in Equation (15) that the sliding surface is third-order as it includes the third derivative of the error signal which clearly indicates that the proposed scheme is a higher-order sliding mode control scheme where the integral action is used to reduce the chattering effects. In addition to integral action that significantly reduces the chattering effects, the term ψ_p uses the power rate reaching law in which the terms $|\xi|^{\gamma_{i,p}}$ with constants $k_{i,p}$ can ensure low chattering through fast reaching with a finite reaching time of the target states [26].

In order to analyze the convergence of the sliding surface to an equilibrium within a finite-time, it is essential to analyze its dynamic characteristics which can be obtained by taking the derivative of Equation (15) and written as follows:

$$\dot{\sigma}_p = \dot{x}_{3,p} - \psi_p. \tag{18}$$

If $\sigma_p = \dot{\sigma}_p = 0$ for a control signal $v_{eq,p}$, it can be said that the sliding surface (σ_p) converges to the equilibrium point and the closed-loop system converges to this sliding surface in the finite-time for this control signal. By substituting Equation (12) into Equation (18) with neglecting parametric uncertainties (i.e. $\Delta\alpha_\mu$), the equivalent control signal can be written as:

$$\begin{aligned} v_{eq,p} = \frac{1}{\alpha_{1n}} \Bigg\{ & \frac{d^3 i_{der,p}^{ref}}{dt^3} + (\alpha_{2n} + \alpha_{3n}) \frac{d^2 i_{der,p}}{dt^2} \\ & + (\alpha_{4n} + \alpha_{5n} + \alpha_{6n}) \frac{d i_{der,p}}{dt} + \alpha_{7n} i_{der,p} \\ & + \alpha_{8n} \frac{d^2 v_{pcc,p}}{dt^2} + \alpha_{9n} \frac{d v_{pcc,p}}{dt} + \alpha_{1n} v_{pcc,p} - \psi_p \Bigg\}. \end{aligned} \tag{19}$$

The control signal ($v_{eq,p}$) can be obtained from Equation (19) by satisfying the condition $\dot{\sigma}_p = 0$. The equivalent control signal in Equation (19) consists of ψ_p in which this part of the controller eliminates the effects of mismatched disturbances because of measurable disturbances caused by $v_{pcc,p}$ and its derivatives. However, Equation (19) includes the unknown parts (i.e. $\Delta\alpha_\mu$) due to variations in parameters and the control signal will have this unknown term if it is derived from Equation (19). The inclusion of unknown terms in a control signal is not feasible as it cannot be implemented. For this reason, the Lyapunov function is used in order to ensure the global stability of the system in the presence of parametric uncertainties.

The stability of the proposed controller is investigated by formulating the Lyapunov function which in fact defines the energy of the system. The energy or Lyapunov function can be written as:

$$W_p(t) = \frac{1}{2}\sigma_p^2 \geq 0. \tag{20}$$

It is well-known that the derivative of $W_p(t)$ in Equation (20) must be negative definite (i.e. $\dot{W}_p(t) < 0$) or semi-definite (i.e. $\dot{W}_p(t) \leq 0$) in order to ensure the overall stability and robustness of the system using the control law obtained based on the sliding surface $\sigma_p(x)$. The derivative of $W_p(t)$ can be written as follows:

$$\dot{W}_p(t) = \sigma_p \dot{\sigma}_p. \tag{21}$$

By substituting Equation (18) into Equation (21), we have:

$$\dot{W}_p(t) = \sigma_p \{\dot{x}_{3,p} - \psi_p\}. \tag{22}$$

By using Equations (12), (14), and (19), Equation (22) is expanded as follows:

$$\dot{W}_p(t) = \sigma_p \Bigg\{ -\Delta\alpha_1 \alpha_{1n}^{-1} \frac{d^3 i_{der,p}^{ref}}{dt^3} + \left(\Delta\alpha_2 + \Delta\alpha_3 - \Delta\alpha_1\alpha_{1n}^{-1}\right)\frac{d^2 i_{der,p}}{dt^2} + \left(\Delta\alpha_4 + \Delta\alpha_5 + \Delta\alpha_6 - \Delta\alpha_1\alpha_{1n}^{-1}\right)\frac{di_{der,p}}{dt} + \left(\Delta\alpha_7 - \Delta\alpha_1\alpha_{1n}^{-1}\right) i_{der,p} + \left(\Delta\alpha_8 - \Delta\alpha_1\alpha_{1n}^{-1}\right)\frac{d^2 v_{pcc,p}}{dt^2} + \left(\Delta\alpha_9 - \Delta\alpha_1\alpha_{1n}^{-1}\right)\frac{dv_{pcc,p}}{dt} - \Delta\alpha_1\alpha_{1n}^{-1} v_{pcc,p} + \Delta\alpha_1\alpha_{1n}^{-1}\psi_p \Bigg\} - \sigma_p(x)\left(1 + \Delta\alpha_1\alpha_{1n}^{-1}\right) v_{r,p}, \tag{23}$$

where $(\cdot)^{-1} = \frac{1}{(\cdot)}$. To satisfy the Lyapunov stability condition, it is essential that Equation (23) be less than or equal to zero, therefore, to find the stability-instability boundrary, the reaching control signal can be written as follows:

$$v_{r,p} = tanh(\sigma_p)(1 + \Delta\alpha_1\alpha_{1n}^{-1})^{-1} \Bigg\{ |-\Delta\alpha_1\alpha_{1n}^{-1}| \left|\frac{d^3 i_{der,p}^{ref}}{dt^3}\right| + |\Delta\alpha_2 + \Delta\alpha_3 - \Delta\alpha_1\alpha_{1n}^{-1}| \left|\frac{d^2 i_{der,p}}{dt^2}\right| + |\Delta\alpha_4 + \Delta\alpha_5 + \Delta\alpha_6 - \Delta\alpha_1\alpha_{1n}^{-1}| \left|\frac{di_{der,p}}{dt}\right| + |\Delta\alpha_7 - \Delta\alpha_1\alpha_{1n}^{-1}| |i_{der,p}| + |\Delta\alpha_8 - \Delta\alpha_1\alpha_{1n}^{-1}| \left|\frac{d^2 v_{pcc,p}}{dt^2}\right| + |\Delta\alpha_9 - \Delta\alpha_1\alpha_{1n}^{-1}| \left|\frac{dv_{pcc,p}}{dt}\right| + |-\Delta\alpha_1\alpha_{1n}^{-1}||v_{pcc,p}| + |\Delta\alpha_1\alpha_{1n}^{-1}||\psi_p| \Bigg\}, \tag{24}$$

where $tanh(\sigma_p)$ is a smooth switching function which operates similar to signum funtion and significantly decreases chattering effects compared to signum function [27]. Equation (24) is simplified as follows by considering Equation (13) and assuming $\varepsilon_1 = \varepsilon_2 = \cdots = \varepsilon_9 = \varepsilon$,

$$v_{r,p} = tanh(\sigma_p)\frac{\varepsilon}{100+\varepsilon} \Bigg\{ \left|\frac{d^3 i_{der,p}^{ref}}{dt^3}\right| + |\alpha_{2n} + \alpha_{3n} - 1| \left|\frac{d^2 i_{der,p}}{dt^2}\right| + |\alpha_{4n} + \alpha_{5n} + \alpha_{6n} - 1| \left|\frac{di_{der,p}}{dt}\right| + |\alpha_{7n} - 1||i_{der,p}| + |\alpha_{8n} - 1| \left|\frac{d^2 v_{pcc,p}}{dt^2}\right| + |\alpha_{9n} - 1| \left|\frac{dv_{pcc,p}}{dt}\right| + |v_{pcc,p}| + |\psi_p| \Bigg\}. \tag{25}$$

In order to determine the controller gain, the worst case is considered in which the maximum values are considered for voltage and current signals. By considering $v_{pcc,p}(t) = \sqrt{2}V_{rms}\sin(\omega t)$ per phase, the reference current signal is determined by $i_{der,p}(t) = i_{der,p}^{ref}(t) = \sqrt{2}I_{rms}\sin(\omega t)$ that I_{rms} is obtained by $I_{rms} = S_n V_{rms}^{-1}$ per phase in which S_n is the nominal rating power of the system per phase.

$$v_{r,p} = tanh(\sigma_p)\frac{\sqrt{2}\varepsilon}{100+\varepsilon} \Bigg\{ |\omega^3 + (\alpha_{2n} + \alpha_{3n} - 1)\omega^2 + (\alpha_{4n} + \alpha_{5n} + \alpha_{6n} - 1)\omega + (\alpha_{7n} - 1)|I_{rms} + |(\alpha_{8n} - 1)\omega^2 + (\alpha_{9n} - 1)\omega + 1|V_{rms} + \frac{|\psi_p|}{\sqrt{2}} \Bigg\}. \tag{26}$$

In order to increase the stability origin of the proposed controller, ε is replaced by $\varepsilon_{\max}$ and the controller gain is considered $(100 + \varepsilon_{\max})$ time bigger than the calculated gain in Equation (26). By considering this subject, the reaching control signal is achieved as follows:

$$v_{r,p} = \lambda_{r,p} tanh(\sigma_p), \tag{27}$$

where,

$$\lambda_{r,p} = \sqrt{2}\varepsilon_{max} \Bigg\{ |\omega^3 + (\alpha_{2n} + \alpha_{3n} - 1)\omega^2 + (\alpha_{4n} + \alpha_{5n} + \alpha_{6n} - 1)\omega + (\alpha_{7n} - 1)|I_{rms} + |(\alpha_{8n} - 1)\omega^2 + (\alpha_{9n} - 1)\omega + 1|V_{rms} + \frac{|\psi_p|}{\sqrt{2}} \Bigg\}. \tag{28}$$

From the above analysis, it can be seen that $\dot{W}_p(t)$ is negative semi-definite. By substituting Equations (19) and (27) into (14), the final control law is achieved as follows:

$$v_{t,p} = \frac{1}{\alpha_{1n}} \Bigg\{ \frac{d^3 i_{der,p}^{ref}}{dt^3} + (\alpha_{2n} + \alpha_{3n})\frac{d^2 i_{der,p}}{dt^2} + (\alpha_{4n} + \alpha_{5n} + \alpha_{6n})\frac{di_{der,p}}{dt} + \alpha_{7n} i_{der,p} + \alpha_{8n}\frac{d^2 v_{pcc,p}}{dt^2}$$

$$+\alpha_{9n}\frac{dv_{pcc,p}}{dt}+\alpha_{1n}v_{pcc,p}-\psi_p+\lambda_p tanh(\tau_p\sigma_p)\Big\}. \quad (29)$$

It is worthy to note than Equation (19) has an additional factor $\frac{1}{\alpha_{1n}}$ while Equation (27) does not have this term, therefore, by substituting these two equations into Equation (14), a factor α_{1n} must be multiplied into (27) if we would include all of the terms into one bracket, which is equalled to λ_p in Equation (29) and is identical as follows:

$$\lambda_p=\alpha_{1n}\lambda_{r,p}. \quad (30)$$

For the three-phases inverter, $v_{t,p}=m_{t,p}\frac{V_{dc}}{2}$ where $m_{t,p}$ is the modulation signal for the inverter. This control signal will ensure the convergence of the sliding surface to the equilibrium point for which the closed-loop system will also converge to the sliding surface in the finite-time. The control signal in Equation (29) includes the derivative terms (up to the second-order) and the computation of these derivatives will introduce noises or disturbances. As the proposed structure includes an LCL filters, some effects of these noises will be eliminated through this filter. Furthermore, the proposed scheme uses a higher-order sliding surface which overcomes the chattering problems due to the excitement of unmodeled dynamics and the effects of such chattering problems are more prominent than that of the noises or disturbances due to the derivatives of i_{der} and v_{pcc} in Equation (29). The control signal as presented by Equation (29) clearly shows that it is independent of the grid voltage and any distortion in the grid voltage will not affect the performance of the controller. Moreover, the proposed scheme is robust against parametric uncertainties. Hence, it will improve the THD with changes in parameters and distortions in the grid voltage. As this control signal is employed for the current control in a grid-connected DER, it is essential to analyze the stability of the system as discussed in the following subsection.

3.4 | Stability analysis

In order to investigate the stability of the proposed controller, Lyapunov function is used as early explained. By using Equations (12) and (29) and substituting them into Equation (22) by considering uncertainties in Equation (13), $\dot{W}_p(t)$ is written as follows:

$$\dot{W}_p(t)=\sigma_p\frac{1}{100}\Bigg\{-\varepsilon_1\frac{d^3i_{der,p}^{ref}}{dt^3}+(\varepsilon_2\alpha_{2n}+\varepsilon_3\alpha_{3n}-\varepsilon_1)\frac{d^2i_{der,p}}{dt^2}+(\varepsilon_4\alpha_{4n}+\varepsilon_5\alpha_{5n}+\varepsilon_1\alpha_{6n}-\varepsilon_1)\frac{di_{der,p}}{dt}+(\varepsilon_7\alpha_{7n}-\varepsilon_1)i_{der,p}+(\varepsilon_8\alpha_{8n}-\varepsilon_1)\frac{d^2v_{pcc,p}}{dt^2}+(\varepsilon_9\alpha_{9n}-\varepsilon_1)\frac{dv_{pcc,p}}{dt}+(\varepsilon_4\alpha_{1n}-\varepsilon_1)v_{pcc,p}+\varepsilon_1\psi_p\Bigg\}$$
$$-\sigma_p\frac{1}{100}(1+\varepsilon_1)\lambda_p tanh(\sigma_p). \quad (31)$$

Equation (31) is briefly written as follows:

$$\dot{W}_p(t)=\sigma_p(\Delta\alpha_{u,p}-\lambda'_p tanh(\sigma_p)). \quad (32)$$

According to the analysis to calculate the value of $\lambda'_{r,p}$ (which is achieved from $\lambda_{r,p}$ in Equation 28) and considering Equation (13) which shows that $\varepsilon_\mu\le\varepsilon_{\max}$, it can be concluded that;

$$\lambda'_{r,p}\ge|\Delta\alpha_{u,p}|. \quad (33)$$

Therefore, Equation (32) can be analysed as follows by considering Equation (33),

$$\begin{aligned}\dot{W}_p(t)&=\sigma_p(x)\Delta_{u,p}-\lambda_p\sigma_p(x)tanh(\sigma_p)\\&\le\lambda_p\sigma_p-\lambda_p\sigma_p tanh(\sigma_p)\\&\le\lambda_p\sigma_p(1-tanh(\sigma_p)).\end{aligned} \quad (34)$$

As λ'_p is a positive constant, then,

$$\begin{cases}\dot{W}_p(t)=0 & \text{if} \quad \sigma_p\ge0\\ \dot{W}_p(t)<0 & \text{if} \quad \sigma_p<0\end{cases}. \quad (35)$$

Equation (35) is simplified as follows:

$$\dot{W}_p(t)\le0. \quad (36)$$

From Equation (36), it can be seen that $\dot{W}_p(t)$ is negative semi-definite. Therefore, the proposed controller ensures the overall stability of the system and since this controller is designed by considering parametric uncertainties, it is robust against these uncertainties. Considering the proposed control signal in Equation (29), the block diagram of the proposed controller is depicted in Figure 2.

4 | PIL SIMULATION RESULTS AND DISCUSSIONS

The performance of the designed controller is evaluated using PIL simulation studies under different operating conditions. The PIL simulation studies are carried out using MATLAB/Simulink platform for the system as shown in Figure 1

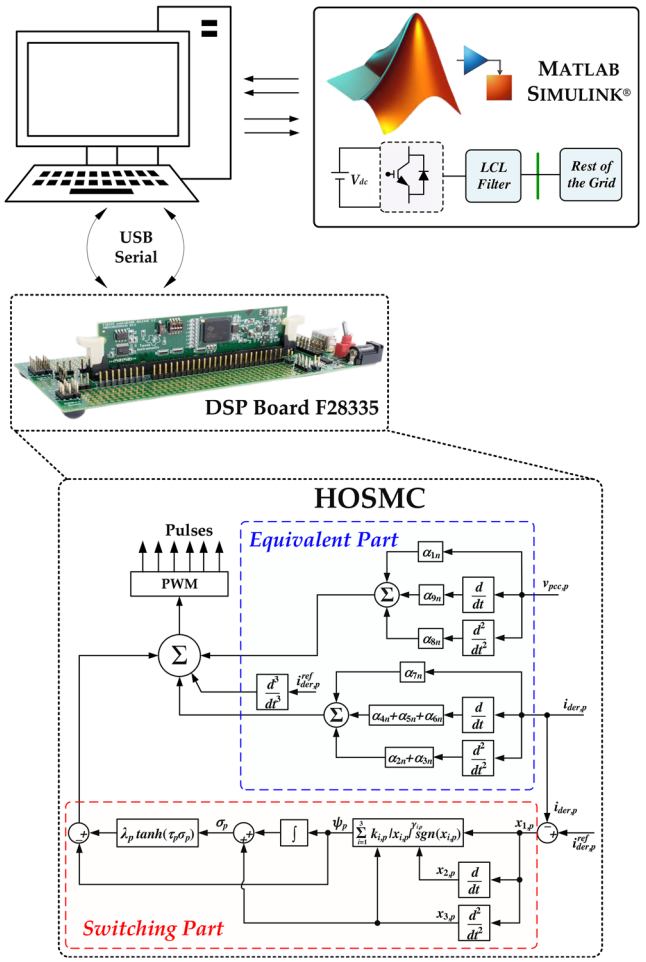

FIGURE 2 Block diagram representation of the proposed control scheme

TABLE 1 Nominal parameters of the system and designed controller for the simulation

Parameter	Value
V_{dc}	400 V
R_{1n}, L_{1n}	0.2 Ω, 2 mH
R_{2n}, L_{2n}	0.16 Ω, 1 mH
C_{fn}	7 μF
ε_μ	30%
R_g, L_g	0.35 Ω, 0.1 mH
Grid voltage (RMS)	110 V
Grid frequency	50 Hz
Switching frequency	10 kHz
λ_p	3.35×10^3
$(k_{1,p}, k_{2,p}, k_{3,p})$	$(4, 2, 7) \times 10^{12}$
$(\gamma_{1,p}, \gamma_{2,p}, \gamma_{3,p})$	$(10, 2.5, 1.7) \times 10^{-3}$

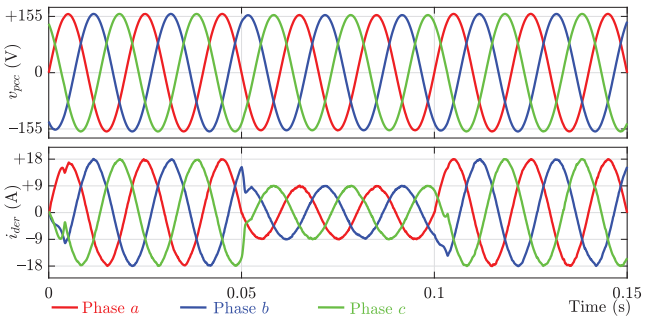

FIGURE 3 The PCC voltage and the current injected into the grid under the normal condition

in which a DSP microcontroller based on TMDSCNCD28335 R2.2 controlCARD is used for running the proposed HOSMC as long as the power circuit including the three-phase inverter along with the interfaced *LCL* filter and the main grid are run in MATLAB/Simulink environment. The main process of this implementation in detail is in such a way that it is directly interlinked to MATLAB/Simulink from which the power system part is run into Simulink environment while the HOSMC part simultaneously is loaded and run into this DSP board via USB. It is worthy to note that in order to implement the controller through USB, the junction J9 must be closed on DSP board. Table 1 lists the nominal values of the system's parameters while the design parameters for the controller are listed in Table 1. To evaluate the performance of the designed controller, two different scenarios considering the following three conditions for the grid voltage are considered:

- Normal condition of the grid voltage,
- Abnormal condition of the grid voltage, and
- Parametric uncertainties on the *LCL* filter.

In the following, these are discussed with the detailed analysis.

4.1 | Case study 1: Performance under the sinusoidal grid voltage condition and the step change in the reference current injected into the grid

In this case, the grid voltage is considered as a sinusoidal waveform and the step change in the reference value of the current injected into the grid is taken into account for evaluating the effectiveness of the designed controller. For this purpose, the reference current injected into the grid is kept to its peak value 18 A from t = 0 s to t = 0.05 s and this peak value changes to 9 A at t = 0.05 s which continues until t = 0.1 s. Finally, the reference current injected into the grid changes to its initial peak value (i.e. 18 A) at t = 0.1 s. This situation is depicted in Figure 3 which illustrates the voltage at the PCC and the changes in the reference current injected into the grid. The responses for the changes in the current injected into the grid include less overshoots while settling down their values to the corresponding reference values. This can also be seen from the response of the errors in the current injected into the grid for all three phases as shown in Figure 4. Hence, it is clear that the designed HOSMC controller operates properly and the actual currents track their corresponding reference values with minimum errors.

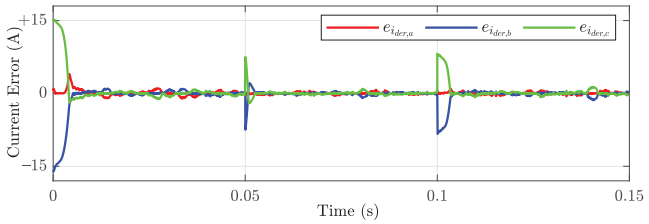

FIGURE 4 The error in the current injected into the grid (i.e. $i_{der}^{ref} - i_{der}$) under the normal condition

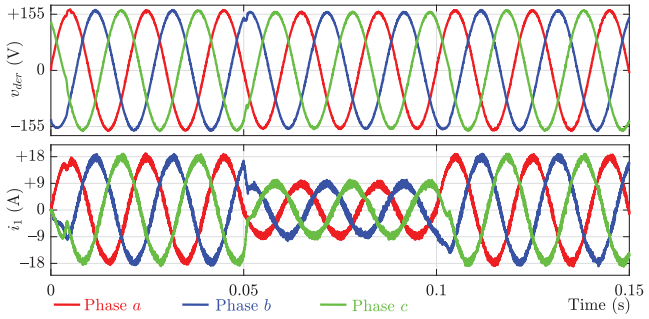

FIGURE 5 The voltages across filter capacitors and inverter-side line currents under the normal condition

Figure 5 shows the responses for voltages across the capacitors in the *LCL* filter and inverter-side line currents. According to these figures, the voltages of the capacitors are almost sinusoidal with less total harmonic distortions as compared to the inverter-side line currents.

4.2 | Case study 2: Performance under unbalanced and distorted grid voltage conditions

In this case study, the performance of the designed controller is evaluated for distorted and unbalanced grid voltage condition. The distortion in the voltage and current responses can be defined as the ratio of the root mean square (RMS) amplitude of the response at frequencies higher than the fundamental one and the RMS value of the amplitude at the fundamental frequency which can be written as follows:

$$THD = \frac{\sqrt{A_2^2 + A_3^2 + A_4^2 + \cdots}}{A_1}, \tag{37}$$

where A_1 is the amplitude at the fundamental frequency and A_i with $i > 1$ represents amplitudes higher than fundamental frequencies. On the other hand, the total demand distortion (TDD) is defined as equal as to THD when the system is operating in its nominal power (i.e. under maximum demand load current) and is a better index compared to THD. It is worthy to note that in order to evaluate the proposed controller in terms of THD, the tested system will be considered under rated power operation which actually define the TDD. The value of the THD

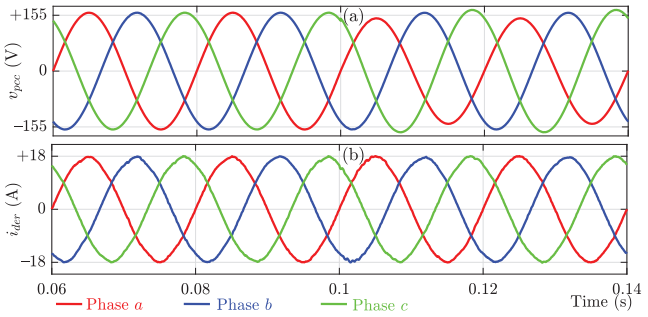

FIGURE 6 The PCC voltage and waveforms for the current under balanced and unbalanced grid voltages

can also be calculated using the fast Fourier transforms (FFTs). To evaluate the performance of the designed controller, the phase voltages of the grid are considered as follows:

- t = 0 s to t = 0.1 s: the grid voltages are completely balanced and almost sinusoidal with the RMS value of 110 V.
- t = 0.1 s to t = 0.2 s: the grid voltages are changed to the unbalanced condition at t = 0.1 s where the per unit (pu) values of three different phases (i.e. *a*, *b*, and *c*) are considered as 0.8, 1, and 1.1 by considering the nominal RMS value of the grid voltage as 110 V.
- t = 0.2 s to t = 0.3 s: the grid voltages are balanced with high harmonic components where the grid voltages are polluted with the 5^{th}, 7^{th}, 11^{th}, and 13^{th} with the amount of 20%, 20%, 10% , and 10% of the main grid voltage (i.e. 110 V) and the corresponding THD of these components yields 31.62%.
- t = 0.3 s to t = 0.4 s: the grid voltages are unbalanced with high harmonic components where the grid voltages are polluted with the 5^{th}, 7^{th}, 11^{th}, and 13^{th} with the amount of 20%, 20%, 10% , and 10% of the main grid voltage (i.e. 110 V).

The PIL simulation results highlight the fully balanced and unbalanced conditions as discussed through the first two points, that is, for the time steps t = 0 s to t = 0.1 s and t = 0.1 s to t = 0.2 s are shown Figure 6 (though only a portion of both steps are shown here for the clear visibility). These results include the voltage at the PCC and the current injected into the grid for all three phases. From Figure 6a, it can be seen that the grid voltage is balanced up to t = 0.1 s while the imbalances in these voltages start from t = 0.1 s. However, the responses for the current injected to the grid are balanced under both balanced and unbalanced grid voltage conditions which can be clearly seen from Figure 6b. Furthermore, there are less transients in these current due to the imbalances in the grid voltages.

The PIL simulation results for the balanced grid voltages but under harmonic conditions are shown in Figure 7 which includes the PCC voltages the current injected into the grid. Figure 7 shows the combined results for both balanced and unbalanced conditions with harmonic distortions. The grid voltages for different phases under these circumstances are shown in Figure 7a and the current injected to the grid are shown in Figure 7b. From Figure 7b, can be clearly shown that the current responses for different phases are almost sinusoidal and

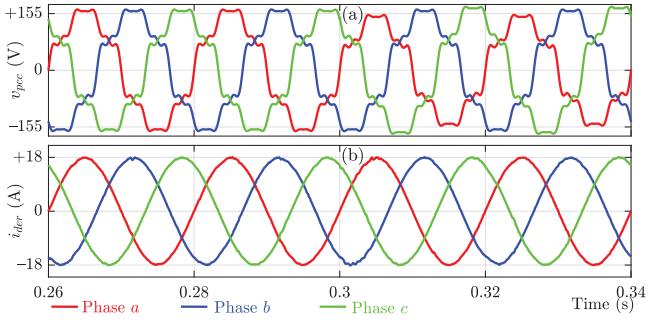

FIGURE 7 The PCC voltage and waveforms for the current under balanced and unbalanced grid voltages with different harmonic components

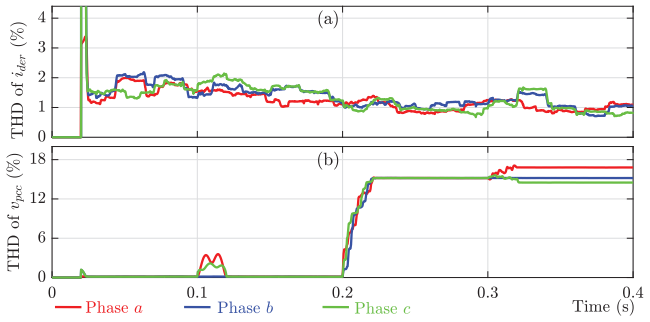

FIGURE 8 THDs under different grid voltage conditions: (a) the THD in the current injected into the grid and (b) the THD in the PCC voltage

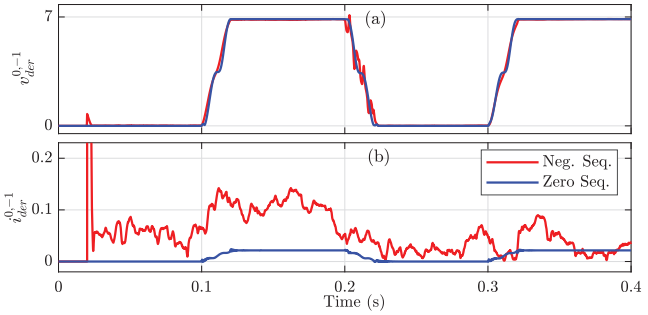

FIGURE 9 The zero and negative sequence components of the PCC voltage and current injected into the grid under different grid voltage conditions

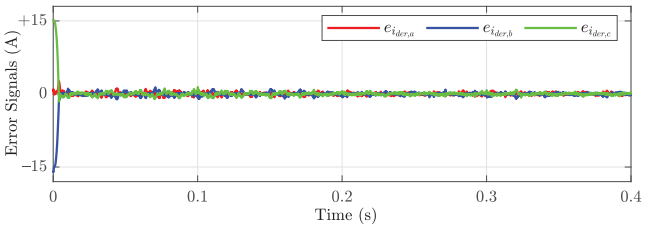

FIGURE 10 The error in the current injected into the grid (i.e. $i_{der}^{ref} - i_{der}$) under different grid voltage conditions

balanced for both balanced and unbalanced grid voltages with different harmonic components.

To further illustrate the performance of the designed HOSMC controller in terms of the THD, the FFTs are carried out for the PCC voltage and current injected into the grid as shown in Figure 8. Figure 8a shows the THD for the current injected into the grid through each phase while Figure 8b shows the same for the PCC voltage. Figure 8a clearly shows that the THD in the currents through each phase is almost lower than 1.5% under any grid voltage condition. From Figure 8b, it can be seen that the designed HOSMC reduces the THD from 31.62% to almost 18% which is a significant improvement.

The zero and negative sequence components of the PCC voltage and the current injected into the grid are shown in Figure 9 in order to further demonstrate the effectiveness of the designed controller. From Figure 9a, it is clear that the negative and zero sequence components of the PCC voltage become unbalanced during two time intervals where the levels of imbalances are around 7%. However, the zero and negative sequence components of the current injected into the grid do not experience any severe unbalances which can also be seen from Figure 9b. This can also be clarified for the tracking capability of the designed HOSMC and it is found that the design controller exhibits very low tracking error for the current injected into the grid. Figure 10 shows the tracking errors in the current injected into the grid through different phases tend to zero under any grid voltage condition.

Table 2 shows the comparison of the designed HOSMC with different existing methods along with the associated parameters. From this table, it can be seen that the designed controller has the lowest THD in the grid current as compared to other controllers. Furthermore, the Park or Clark transformations increase the complexities during the implementation of most existing controllers while the designed HOSMC does not use any of these transformations. Table 2 also shows that the designed HOSMC requires more measurement sensors in the natural frame than that of an SMC+PR controller in the similar frame. However, the SMC+PR controller in the reference frame needs a larger switching frequency in order to achieve similar performance to that of the designed HOSMC which definitely increases the power losses and hence, decreases the whole lifetime of the converter. With the decrease in the switching frequency for the SMC+PR controller in the reference frame, it is required to utilize the large values for filters' parameters. Finally, it can be summarized that the designed controller efficiently rejects the effects of uncertainties and disturbances which also enables to reduce the harmonics in the PCC voltage.

4.3 | Case study 3: Performance under the filter parametric uncertainties and distorted grid voltage conditions

In order to investigate the robustness of the proposed controller against the filter parametric uncertainties, a −30% parametric variation is practised on the system for which the values of *LCL* filter are reduced to 70% of their nominal values while the employed values through the controller loop are remained to the nominal values without any re-setting. In this scenario, firstly, the parameters of the filter are remained in their own nominal

TABLE 2 Comparisons of different control methods in the grid-connected mode of inverter

Comparison category	SMHC [14]	SMC+PR (Rotating *dq* form) [15]	SMC+PR (Natural frame) [15]	DTSMC [16]	IM-based [28]	SMC+KFE [17]	HOSMC
Type of the filter	*L*	*LCL*	*LCL*	*LCL*	*LCL*	*LCL*	*LCL*
V_{dc} (V)	420	600	600	–	340	450	400
L_1/L_2 (mH)	7/NA	1.74/0.6867	1.74/0.6867	1/0.3	1.7/0.6	7/5	2/1
R_1/R_1 (Ω)	0.5/NA	0.2/0.076	0.2/0.076	0.5/0.5	0.5/0.3	–	0.2/0.16
C_f (μF)	–	10	10	62	4.5	6.8	7
L_g (mH)	–	–	–	1	1.2	0.8	0.1
Switching frequency (kHz)	10	125	125	12	10	6	10
Grid voltage in RMS (V)	220	230	230	110	127	110	110
Grid frequency (Hz)	60	60	60	60	60	60	50
THD in the grid current (%)	2.25	1.8	1.3	–	3.29	–	<1.5
Number of voltage measurements	3	3	2	6	3	3	3
Number of current measurements	3	3	2	6	3	3	3
Park/Clark transformation	Required	Required	Not required	Required	Required	Not required	Not required
Inverse Park/Clark transformation	Required	Required	Not required	Required	Not required	Not required	Not required
Complexity	Moderate	Moderate	Simple	Moderate	Moderate	Simple	Moderate

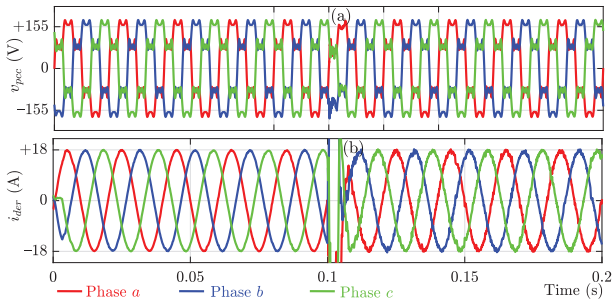

FIGURE 11 The PCC voltage and waveforms for the current under parametric uncertainties

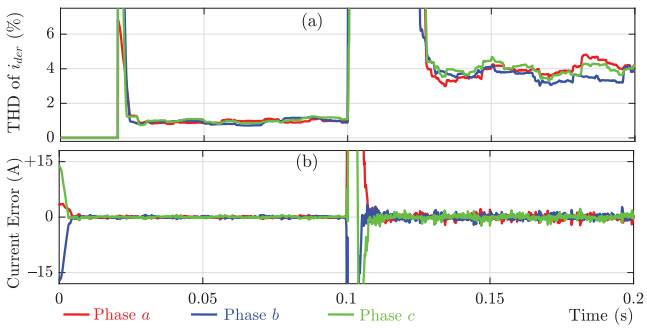

FIGURE 12 The error in the current injected into the grid (i.e. $i_{der}^{ref} - i_{der}$) under parametric uncertainties

values while they are finally diminished into their new values by a switching action at t = 0.1 s. The implementation results under parametric uncertainties' circumstances through the PIL are represented in Figures 11 and 12 for the PCC voltage as long as current waveforms and the current THD as well as its errors' waveforms, respectively. Figure 11a shows the PCC-side voltage with penetration of highly harmonic components as case study 2 circumstances under balanced voltage waveforms from which the corresponding output-side current waveforms are demonstrated in Figure 11b and the results show that the system is still stable with a slightly altering in current waveforms after parametric uncertainties' occurring. As Figure 12a displays, the THDs of the output-side currents are slightly higher under the worst condition of the grid voltages' harmonic existence and highly parametric uncertainties that can be figured out that the proposed HOSMC is still remained robust against filter parameters' variations. Furthermore, Figure 12b exhibits the error signals of the output current waveforms for all of three phases from where it is vivid that these error signals are still indicating the better performance of the presented HOSMC approach.

5 | CONCLUSION

A robust nonlinear current controller is designed for grid-connected three-phase inverter-interfaced distributed generators using the higher-order concept of the sliding mode control strategy. The current controller is designed to ensure robustness against parametric uncertainties where these uncertainties are modeled based on the Taylor series expansion method and the stability of the designed controller is analyzed by formulating the Lyapunov function. The PIL simulation studies are carried out to validate the performance against parametric uncertainties including disturbances in grid voltages, for example, unbalances and harmonics in the grid voltage. Simulation results clearly depict that the designed higher-order sliding mode controller efficiently tracks the current and significantly reduces the harmonics under any operating condition. The designed controller

keeps the total harmonic distortion in the current injected into the grid lower than 1% and the same in the grid voltage from 32.16% to 18% for the PIL simulation results. The validations through PIL results show that the harmonics in the current injected into the grid and the PCC voltages exhibit similar characteristics to that of PIL simulation results. One of the major characteristics of the proposed HOSMC is that while the equilibrium point of the system is altered, there will be no necessity for tuning the parameters. In addition, the fast response to different disturbances is another main advantage of this controller. However, most of the traditional SMCs suffer from chattering phenomena while the proposed HOSMC is able to reduce these high frequency components from the control signal. But there is still a drawback of no fixed switching frequency which can be further investigated as a future trend. In this work, the harmonic of the grid voltage is still bit higher as the grid voltages are initially polluted with severe harmonics. In future, the designed controller will be implemented on a large-scale system in decentralized and distributed manners. Future work will also consider the dynamics of the PLL to design a similar controller and analyze the performance by considering unbalances and disturbances in the grid voltage and frequency. On the other hand, it is well-known that there are some disturbances from the input side due to natural features of renewable energy resources, which make uncertainties on the input DC voltage source and requires more investigations as an another future work.

DATA AVAILABILITY STATEMENT

The data that support the findings of this study are available on request from the corresponding author. The data are not publicly available due to privacy or ethical restrictions.

CONFLICT OF INTEREST

The authors do not have any conflict of interests.

ORCID

Mostafa Barzegar-Kalashani https://orcid.org/0000-0003-1942-9416
Behrouz Tousi https://orcid.org/0000-0002-1215-1071
Md Apel Mahmud https://orcid.org/0000-0002-5302-5338
Mohammad Farhadi-Kangarlu https://orcid.org/0000-0002-3827-2058

REFERENCES

1. Blaabjerg, F., Chen, Z., Kjaer, S.B.: Power electronics as efficient interface in dispersed power generation systems. IEEE Trans. Power Electron. 19(5), 1184–1194 (2004)
2. Hossain, J., Mahmud, A.: Renewable energy integration: Challenges and solutions. Springer Science & Business Media, Singapore (2014)
3. Beres, R.N., Wang, X., Liserre, M., Blaabjerg, F., Bak, C.L.: A review of passive power filters for three-phase grid-connected voltage-source converters. IEEE J. Emerging Sel. Topics Power Electron. 4(1), 54–69 (2016)
4. Lettl, J., Bauer, J., Linhart, L.: Comparison of different filter types for grid connected inverter. PIERS Proceedings. IEEE, Piscataway (2011)
5. Serpa, L.A., Ponnaluri, S., Barbosa, P.M., Kolar, J.W.: A modified direct power control strategy allowing the connection of three-phase inverters to the grid through *LCL* filters. IEEE Trans. Ind. Appl. 43(5), 1388–1400 (2007)
6. Pan, D., Ruan, X., Bao, C., Li, W., Wang, X.: Capacitor-current-feedback active damping with reduced computation delay for improving robustness of LCL-type grid-connected inverter. IEEE Trans. Power Electron. 29(7), 3414–3427 (2014)
7. Twining, E., Holmes, D.G.: Grid current regulation of a three-phase voltage source inverter with an *LCL* input filter. IEEE Trans. Power Electron. 18(3), 888–895 (2003)
8. Jia, Y., Zhao, J., Fu, X.: Direct grid current control of *LCL*-filtered grid-connected inverter mitigating grid voltage disturbance. IEEE Trans. Power Electron. 29(3), 1532–1541 (2014)
9. Xu, J., Tang, T., Xie, S.: Research on low-order current harmonics rejections for grid-connected *LCL*-filtered inverters. IET Power Electron. 7(5), 1227–1234 (2014)
10. Papavasiliou, A., Papathanassiou, S.A., Manias, S.N., Demetriadis, G.: Current control of a voltage source inverter connected to the grid via *LCL* filter. In: 2007 IEEE Power Electronics Specialists Conference, pp. 2379–2384. IEEE, Piscataway (2007)
11. Liu, T., Hao, X., Yang, X., Zhao, M., Huang, Q., Huang, L.: A novel repetitive control scheme for three-phase grid-connected inverter with *LCL* filter. In: Proceedings of the 7th International Power Electronics and Motion Control Conference, vol. 1, pp. 335–339. IEEE, Piscataway (2012)
12. Hao, X., Yang, X., Liu, T., Huang, L., Chen, W.: A sliding-mode controller with multiresonant sliding surface for single-phase grid-connected VSI with an *LCL* filter. IEEE Trans. Power Electron. 28(5), 2259–2268 (2013)
13. Komurcugil, H., Ozdemir, S., Sefa, I., Altin, N., Kukrer, O.: Sliding-mode control for single-phase grid-connected *LCL*-filtered VSI with double-band hysteresis scheme. IEEE Trans. Ind. Electron. 63(2), 864–873 (2016)
14. Kang, S., Kim, K.: Sliding mode harmonic compensation strategy for power quality improvement of a grid-connected inverter under distorted grid condition. IET Power Electron. 8(8), 1461–1472 (2015)
15. Altin, N., Ozdemir, S., Komurcugil, H., Sefa, I.: Sliding-mode control in natural frame with reduced number of sensors for three-phase grid-tied *LCL*-interfaced inverters. IEEE Trans. Ind. Electron. 66(4), 2903–2913 (2019)
16. Vieira, R.P., Martins, L.T., Massing, J.R., Stefanello, M.: Sliding mode controller in a multiloop framework for a grid-connected VSI with *LCL* filter. IEEE Trans. Ind. Electron. 65(6), 4714–4723 (2018)
17. Guzman, R., de Vicuña, L.G., Castilla, M., Miret, J., Martín, H.: Variable structure control in natural frame for three-phase grid-connected inverters with *LCL* filter. IEEE Trans. Power Electron. 33(5), 4512–4522 (2018)
18. Barzegar Kalashani, M., Tousi, B., Mahmud, M.A., Farhadi Kangarlu, M.: Robust nonlinear sliding mode controllers for single-phase inverter interfaced distributed energy resources based on super twisting algorithms. Accepted for Publication in ISA Transactions (May 2021)
19. Laghrouche, S., Plestan, F., Glumineau, A.: Higher order sliding mode control based on integral sliding mode. Automatica 43(3), 531–537 (2007)
20. Zong, Q., Zhao, Z., Zhang, J.: Brief paper: Higher order sliding mode control with self-tuning law based on integral sliding mode. IET Control Theory Appl. 4(7), 1282–1289 (2010)
21. Wu, Y., Huangfu, Y., Ma, R., Ravey, A., Chrenko, D.: A strong robust DC-DC converter of all-digital high-order sliding mode control for fuel cell power applications. J. Power Sources 413, 222–232 (2019)
22. Mondal, S., Mahanta, C.: Adaptive integral higher order sliding mode controller for uncertain systems. J. Control Theory Appl. 11(1), 61–68 (2013)
23. Barzegar Kalashani, M., Tousi, B., Mahmud, M.A., Farhadi Kangarlu, M.: Non-linear integral higher-order sliding mode controller design for islanded operations of T-type three-phase inverter-interfaced distributed energy resources. IET Gener. Transm. Distrib. 14(1), 53–61 (2020)
24. Sun, Y., de Jong, E., Wang, X., Yang, D., Blaabjerg, F., Cuk, V., et al.: Sun, Y., et al.: The impact of PLL dynamics on the low inertia power grid: A case study of bonaire island power system. Energies 12(7), 1259 (2019)
25. Bhat, S.P., Bernstein, D.S.: Geometric homogeneity with applications to finite-time stability. Math. Control, Signals Syst. 17(2), 101–127 (2005)
26. Gao, W., Hung, J.C.: Variable structure control of nonlinear systems: a new approach. IEEE Trans. Ind. Electron. 40(1), 4–55 (1993)
27. Aghababa, M.P., Akbari, M.E.: A chattering–free robust adaptive sliding mode controller for synchronization of two different chaotic systems with

unknown uncertainties and external disturbances. Appl. Math. Comput. 218(9), 5757–5768 (2012)
28. Lai, N., Kim, K.: Robust control scheme for three-phase grid-connected inverters with *LCL*-filter under unbalanced and distorted grid conditions. IEEE Trans. Energy Convers. 33(2), 506–515 (2018)

How to cite this article: Barzegar-Kalashani M., Tousi B., Mahmud M.A., Farhadi-Kangarlu M. Higher-order sliding mode current controller for grid-connected distributed energy resources with *LCL* filters under unknown grid voltage conditions. IET Gener. Transm. Distrib. 1–15 (2022).
https://doi.org/10.1049/gtd2.12384

APPENDIX A: TAYLOR SERIES EXPANSION OF UNCERTAIN TERMS

Equation (11) includes different terms which model parameter uncertainties and variations in the *LCL* filter. The details for simplifying these terms are discussed in the following:

- First uncertainty term (α_1) in Equation (11)
The first uncertainty term (α_1) can be represented as follows:

$$\alpha_1 = \frac{1}{(L_{1n} + \Delta L_1)(L_{2n} + \Delta L_2)(C_{fn} + \Delta C_f)}, \tag{A1}$$

which can be simplified as

$$\alpha_1 = \frac{1}{L_{1n}L_{2n}C_{fn}} \frac{1}{1 + \Delta_1}, \tag{A2}$$

with

$$\Delta_1 = \frac{\Delta L_1}{L_{1n}} + \frac{\Delta L_2}{L_{2n}} + \frac{\Delta C_f}{C_{fn}} \frac{\Delta L_1 \Delta L_2}{L_{1n}L_{2n}} + \frac{\Delta L_1 \Delta C_f}{L_{1n}C_{fn}} + \frac{\Delta L_2 \Delta C_f}{L_{2n}C_{fn}} + \frac{\Delta L_1 \Delta L_2 \Delta C_f}{L_{1n}L_{2n}C_{fn}}. \tag{A3}$$

By employing the Taylor series expansion method, Equation (A2) can be expanded as:

$$\alpha_1 = \frac{1}{L_{1n}L_{2n}C_{fn}} + \Delta\alpha_1 = \alpha_{1n} + \Delta\alpha_1, \tag{A4}$$

with

$$\Delta\alpha_1 = \frac{1}{L_{1n}L_{2n}C_{fn}}(-\Delta_1 + \Delta_1^2 - \cdots). \tag{A5}$$

In Equation (A4), it is worth to note that $\frac{1}{L_{1n}L_{2n}C_{fn}}$ and $\Delta\alpha_1$ are the nominal and unknown parts of the parameters and corresponding uncertainties, respectively. The similar approach can be used for all other remaining uncertainty terms in Equation (11) which can be expressed in the form of nominal and unknown parts. Furthermore, as the variable part of ΔL_1 divided to its nominal value, that is, L_{1n}, it is clear that ΔL_1 is smaller that L_{1n}. Regarding to this subject, Δ_1 will be lower than 1, that is, $\Delta_1 < 1$. It is worthy to note that this condition can be considered for the other following terms.

- Second uncertainty term (α_2) in Equation (11)
The second uncertainty term (α_2) can be written as follows:

$$\alpha_2 = \frac{(R_{1n} + \Delta R_1)}{(L_{1n} + \Delta L_1)} = \frac{R_{1n}}{L_{1n}} \frac{1}{1 + \Delta_2} + \Delta_3, \tag{A6}$$

where

$$\Delta_2 = \frac{\Delta L_1}{L_{1n}}, \tag{A7}$$

and

$$\Delta_3 = \frac{\Delta R_1}{L_{1n} + \Delta L_1}. \tag{A8}$$

By using the Taylor series expansion method, Equation (A6) can be expressed as follows:

$$\alpha_2 = \frac{R_{1n}}{L_{1n}} + \Delta\alpha_2 = \alpha_{2n} + \Delta\alpha_2, \tag{A9}$$

with

$$\Delta\alpha_2 = \frac{R_{1n}}{L_{1n}}(-\Delta_2 + \Delta_2^2 - \cdots) + \Delta_3. \tag{A10}$$

- Third uncertainty term (α_3) in Equation (11)
The third uncertainty term (α_3) in Equation (11) can be written as follows:

$$\alpha_3 = \frac{(R_{2n} + \Delta R_2)}{(L_{2n} + \Delta L_2)} = \frac{R_{2n}}{L_{2n}} \frac{1}{1 + \Delta_4} + \Delta_5, \tag{A11}$$

with

$$\Delta_4 = \frac{\Delta L_2}{L_{2n}}, \tag{A12}$$

and

$$\Delta_5 = \frac{\Delta R_2}{L_{2n} + \Delta L_2}. \tag{A13}$$

By using the Taylor series expansion method, Equation (A11) can be expanded as

$$\alpha_3 = \frac{R_{2n}}{L_{2n}} + \Delta\alpha_3 = \alpha_{3n} + \Delta\alpha_3, \tag{A14}$$

with

$$\Delta\alpha_3 = \frac{R_{2n}}{L_{2n}}(-\Delta_4 + \Delta_4^2 - \cdots) + \Delta_5. \quad \text{(A15)}$$

- Fourth uncertainty term (α_4) in Equation (11)
The fourth uncertainty term (α_4) in Equation (11) can be written as follows:

$$\alpha_4 = \frac{1}{(L_{1n} + \Delta L_1)(C_{fn} + \Delta C_f)}, \quad \text{(A16)}$$

which can be simplified as

$$\alpha_4 = \frac{1}{L_{1n}C_{fn}}\frac{1}{1+\Delta_6}, \quad \text{(A17)}$$

with

$$\Delta_6 = \frac{\Delta L_1}{L_{1n}} + \frac{\Delta C_f}{C_{fn}} + \frac{\Delta L_1 \Delta C_f}{L_{1n}C_{fn}}. \quad \text{(A18)}$$

The Taylor series expansion method will expand Equation (A17) as:

$$\alpha_4 = \frac{1}{L_{1n}C_{fn}} + \Delta\alpha_4 = \alpha_{4n} + \Delta\alpha_4, \quad \text{(A19)}$$

with

$$\Delta\alpha_4 = \frac{1}{L_{1n}C_{fn}}(-\Delta_6 + \Delta_6^2 - \cdots). \quad \text{(A20)}$$

- Fifth uncertainty term (α_5) in Equation (11)
The fifth uncertainty term (α_5) in Equation (11) can be written as follows:

$$\alpha_5 = \frac{1}{(L_{2n} + \Delta L_2)(C_{fn} + \Delta C_f)} = \frac{1}{L_{2n}C_{fn}}\frac{1}{1+\Delta_7}, \quad \text{(A21)}$$

which can be simplified as

$$\alpha_5 = \frac{1}{L_{2n}C_{fn}}\frac{1}{1+\Delta_7}, \quad \text{(A22)}$$

with

$$\Delta_7 = \frac{\Delta L_2}{L_{2n}} + \frac{\Delta C_f}{C_{fn}} + \frac{\Delta L_2 \Delta C_f}{L_{2n}C_{fn}}. \quad \text{(A23)}$$

By using the Taylor series expansion method, Equation (A22) can be expanded as follows:

$$\alpha_5 = \frac{1}{L_{2n}C_{fn}} + \Delta\alpha_5 = \alpha_{5n} + \Delta\alpha_5, \quad \text{(A24)}$$

with

$$\Delta\alpha_5 = \frac{1}{L_{2n}C_{fn}}(-\Delta_7 + \Delta_7^2 - \cdots). \quad \text{(A25)}$$

- Sixth uncertainty term (α_6) in Equation (11)
The sixth uncertainty term (α_6) in Equation (11) can be written as follows:

$$\alpha_6 = \frac{(R_{1n} + \Delta R_1)(R_{2n} + \Delta R_2)}{(L_{1n} + \Delta L_1)(L_{2n} + \Delta L_2)} = \frac{R_{1n}R_{2n}}{L_{1n}L_{2n}}\frac{1+\Delta_8}{1+\Delta_9}, \quad \text{(A26)}$$

which can be expressed as:

$$\alpha_6 = \frac{R_{1n}R_{2n}}{L_{1n}L_{2n}}\frac{1+\Delta_8}{1+\Delta_9}, \quad \text{(A27)}$$

with

$$\Delta_8 = \frac{\Delta R_1}{R_{1n}} + \frac{\Delta R_2}{R_{2n}} + \frac{\Delta R_1 \Delta R_2}{R_{1n}R_{2n}}, \quad \text{(A28)}$$

and

$$\Delta_9 = \frac{\Delta L_1}{L_{1n}} + \frac{\Delta L_2}{L_{2n}} + \frac{\Delta L_1 \Delta L_2}{L_{1n}L_{2n}}. \quad \text{(A29)}$$

The Taylor series expansion method will expand Equation (A27) as:

$$\alpha_6 = \frac{R_{1n}R_{2n}}{L_{1n}L_{2n}} + \Delta\alpha_6 = \alpha_{6n} + \Delta\alpha_6, \quad \text{(A30)}$$

with

$$\Delta\alpha_6 = \frac{R_{1n}R_{2n}}{L_{1n}L_{2n}}(\Delta_8 + (1+\Delta_8)(-\Delta_9 + \Delta_9^2 - \cdots)). \quad \text{(A31)}$$

- Seventh uncertainty term (α_7) in Equation (11)
The seventh uncertainty term (α_7) in Equation (11) can be written as follows:

$$\alpha_7 = \frac{(R_{1n} + \Delta R_1) + (R_{2n} + \Delta R_2)}{(L_{1n} + \Delta L_1)(L_{2n} + \Delta L_2)(C_{fn} + \Delta C_f)}, \quad \text{(A32)}$$

which can be simplified as:

$$\alpha_7 = \frac{R_{1n} + R_{2n}}{L_{1n}L_{2n}C_{fn}}\frac{1}{1+\Delta_1} + \Delta_{10}, \quad \text{(A33)}$$

with

$$\Delta_{10} = \frac{\Delta R_1 + \Delta R_2}{(L_{1n} + \Delta L_1)(L_{2n} + \Delta L_2)(C_{fn} + \Delta C_f)}. \quad \text{(A34)}$$

By employing the Taylor series expansion method, Equation (A33) can be written as:

$$\alpha_7 = \frac{R_{1n} + R_{2n}}{L_{1n}L_{2n}C_{fn}} + \Delta\alpha_7 = \alpha_{7n} + \Delta\alpha_7, \tag{A35}$$

with

$$\Delta\alpha_7 = \frac{R_{1n} + R_{2n}}{L_{1n}L_{2n}C_{fn}}(-\Delta_1 + \Delta_1^2 - \cdots) + \Delta_{10}. \tag{A36}$$

- Eighth uncertainty term (α_8) in Equation (11)
  The eighth uncertainty term (α_8) in Equation (11) can be written as follows:

$$\alpha_8 = \frac{1}{L_{2n} + \Delta L_2} = \frac{1}{L_{2n}(1 + \Delta_{11})}, \tag{A37}$$

with

$$\Delta_{11} = \frac{\Delta L_2}{L_{2n}}. \tag{A38}$$

If the Taylor series expansion method is employed on Equation (A37), it can be written as:

$$\alpha_8 = \frac{1}{L_{2n}} + \Delta\alpha_8 = \alpha_{8n} + \Delta\alpha_8, \tag{A39}$$

with

$$\Delta\alpha_8 = \frac{1}{L_{2n}}(-\Delta_{11} + \Delta_{11}^2 - \cdots). \tag{A40}$$

- Ninth uncertainty term (α_9) in Equation (11)

The ninth uncertainty term (α_9) in Equation (11) can be written as follows:

$$\alpha_9 = \frac{R_{1n} + \Delta R_1}{(L_{1n} + \Delta L_1)(L_{2n} + \Delta L_2)}, \tag{A41}$$

which can also be written as:

$$\alpha_9 = \frac{R_{1n}}{L_{1n}L_{2n}(1 + \Delta_{12})} + \Delta_{13}, \tag{A42}$$

with

$$\Delta_{13} = \frac{\Delta R_1}{(L_{1n} + \Delta L_1)(L_{2n} + \Delta L_2)}, \tag{A43}$$

and

$$\Delta_{12} = \frac{\Delta L_1}{L_{1n}} + \frac{\Delta L_2}{L_{2n}}. \tag{A44}$$

By applying the Taylor series expansion method, Equation (A42) can be written as:

$$\alpha_9 = \frac{R_{1n}}{L_{1n}L_{2n}} + \Delta\alpha_9 = \alpha_{9n} + \Delta\alpha_9, \tag{A45}$$

with

$$\Delta\alpha_9 = \frac{R_{1n}}{L_{1n}L_{2n}}(-\Delta_{12} + \Delta_{12}^2 - \cdots) + \Delta_{13}. \tag{A46}$$

In general, that the part associated with uncertainties can be represented as $\Delta\alpha_\mu$ with $\mu = 1, 2, \cdots, 9$.